Published by Avanti Publishers

International Journal of Architectural Engineering Technology

ISSN (online): 2409-9821

Determination of Multiple-target Equivalent Static Wind Load of Large-span Roof Structures based on Clustering Analysis Techniques

Ming-Hui Huang[1], Chung-Lin Fu[2], Yu-Wen Hsu[3], Yuan-Lung Lo[3,*]

[1]Department of Civil Engineering, [2]Wind Engineering Research Center, Tamkang University, New Taipei, Taiwan
[3]Department of Civil Engineering, National Taipei University of Technology, Taipei, Taiwan

ARTICLE INFO

Article Type: Research Article

Guest Editor: *Mariangela De Vita*

Keywords:
Clustering analysis
Inertial force method
Large-span roof structure
Equivalent static wind load
Load-response-correlation method

Timeline:
Received: August 23, 2023
Accepted: November 10, 2023
Published: December 27, 2023

Citation: Huang M-H, Fu C-L, Hsu Y-W, Lo Y-L. Determination of multiple-target equivalent static wind load of large-span roof structures based on clustering analysis techniques. Int J Archit Eng Technol. 2023; 10: 118-139.

DOI: https://doi.org/10.15377/2409-9821.2023.10.9

ABSTRACT

Spatial structures in modern society exhibit a city's distinguishing features and show its strength in building technology. Large-span roof structures are mostly seen among spatial structures for various activities. Large-span roof structures are usually sensitive to wind loads due to their lightness in materials and curved geometric appearance. However, spatial structures are generally designed with many structural members, making it challenging to determine adequate load distributions for structural safety analysis. This paper intends to introduce the concept of the multiple-target equivalent static wind loads and to demonstrate how to reduce the heavy computational burden when the structural designer needs to consider multiple loading effects of the target structure. The wind tunnel test of an elliptical-shaped stadium structure with a flat roof is first conducted to show the fundamental aerodynamic characteristics. The methodologies of the background-component wind force based on the load-response-correlation (LRC) method and the resonant-component wind force based on the inertial force method are then introduced for the specification of single-target equivalent static wind loads. Finally, the clustering analysis technique is adopted to explain the concept of the multiple-target equal static wind loads. A decay index is proposed to indicate how the clustering technique improves the specification of equivalent static wind loads.

*Corresponding Author
Email: yllo@mail.ntut.edu.tw
Tel: +(886) 2-27712171 #2680

1. Introduction

The assessment of the wind-induced response for various structural entities varies due to differences in their structural systems. In the context of rapid economic development, there has been an increasing diversification of structural entities. Generally speaking, engineers can calculate the design wind loads for the target structure based on the formulas specified in the regulations [1-5] for longitudinal, lateral, and torsional forces. With appropriate reliability analysis of specified limit state design scenarios, wind loads are combined with dead loads or live loads in a linear combination format. However, the design parameters for target structures specified in the regulations often tend to be overly idealized. Consequently, when applying the formulas or charts from these regulations to compute wind loads, the results often yield conservative design values. Although current regulations encompass many of the wind characteristics of structures, the formulas provided do not adequately represent all structures, especially those with unique designs that have emerged in recent years. The wind engineering academic community has developed numerous methods related to equivalent design wind loads in recent years, conducting comparative analyses for various structures to discern a universal load calculation method suitable for all structures. Generally, the equivalent design wind loads for tall buildings are predominantly estimated using the Gust Response/Loading Factor Method [6-13]. The primary reasons for this preference are the distinct and evident modal characteristics of tall buildings, the significant separation between vibration modes in the frequency domain, and the high similarity between mean wind forces and the fundamental modal characteristics of tall buildings. However, for some other types of structures, the results estimated using the Gust Response/Loading Factor Method may not be applicable due to the absence of dynamic characteristics in tall buildings [14-17]. A salient example is the wind load calculation approach for large-span roof structures. For some large-span roof structures with relatively high structural frequencies, the resonant response is not pronounced, and the wind pressure distribution exhibits a high degree of spatial correlation. As a result, the Load-Response-Correlation (LRC) Method is typically employed to calculate the background component of the structural response [18-20], or the Universal Equivalent Static Wind Load Method might be utilized [21]. The following paragraph briefly introduces significant literature on equivalent static wind load methods.

In 1967, Davenport introduced the Gust Loading Factor (GLF), a method that determines the equivalent design wind load by multiplying the average wind force by the gust response factor [6]. As the prototype for equivalent design wind loads, the GLF method is limited by its basic assumptions. It is unsuitable for structures with zero cross-wind mean wind force or significant dynamic characteristics. GLF is applied to ensure the equivalent displacement at the rooftop level. However, for high-flexibility long-span roof structures, the wind-induced response and the mass of structural members are related to modal shapes, requiring considerations beyond a single mode, thus conflicting with the GLF method [14-17]. Holmes [22, 23] classified equivalent design wind loads into two parts based on vibration response characteristics: background response with a wide frequency similar to inflow characteristics and resonant response related to the structure's narrow frequency. This method is applicable for understanding equivalent design wind loads for structures with different dynamic characteristics and has become an essential direction for subsequent research. Through wind tunnel experiments, Hongo [24] studied the effect of approaching flow and the geometric shape of dome roofs. An empirical formula was presented to estimate the design wind load for structural members and trusses, considering only the magnitude of the wind load without the effects of dynamic reactions, rendering it suitable only for rigid trusses and members. Uematsu *et al*. [25] conducted wind tunnel experiments on single-layer lattice dome structures, measuring the surface mean wind pressure of nine different high-span ratio models under turbulent boundary layer flow and obtaining the time history of wind load through the orthogonal mode POD method. Holmes [26] addressed the resonant response part of equivalent static wind loads on bridges, identifying that the load distribution and contribution to various structural responses are related to each mode. By employing the orthogonal mode POD method, he calculated the weight factors between modes, with each mode's load proportion to the total load constituting the weight factor. This work also introduced the assumption of inertia force distribution for flutter response, calculating each mode's load response and the equivalent static wind load for bridge resonance. Zhou *et al*. [10-12] pointed out that although the GLF method can accurately estimate displacement response, its predictions for other reactions are suboptimal. Chen and Kareem [14] conducted similar research using Holmes' method [26], demonstrating its applicability in calculating background response loads and comparing it with LRC method results, achieving approximate solutions with multiple mode superpositions. Holmes [23] divided the

equivalent static wind load into background and resonant responses. Given the potential overprediction of these responses, he calculated the weights of both to align them with actual load responses, extending their applicability in design. Davenport [27], Kareem, and Zhou [15] revised the conventional GLF method, making it suitable for estimating different responses through aerodynamic wind load data. This improved GLF method continues to be widely used in architectural wind codes.

Yang [15] applied the LRC method to explore curved roof design wind loads. In LRC design, the equivalent static wind load distribution using the same cylinder connected to four members of the curved roof yielded results close to the actual values. A vital engineering challenge lies in selecting suitable structural response forms based on calculations. Wang [20] employed the LRC method to analyze equivalent static wind loads on buildings with large-span dome structures. By utilizing wind pressure data from wind tunnel experiments on a hemispherical roof structure and converting it into structural node wind forces, a comparison between LRC and wind load time history methods revealed an error margin of around 20%. Lin and Wang [16] developed an equivalent static wind load expression using bridge flutter theory and aerodynamic parameters from wind tunnel experiments, encompassing static and dynamic wind effects. Lo and Wu [17] adopted LRC and Universal methods for equivalent static load analysis, confirming reasonable prediction results with different height and span ratio models. Both methods have shortcomings: while LRC is reasonable, it is time-consuming for more complex degrees of freedom systems, and the Universal method, though quickly reaching over 80% modal energy, does not relate predictions to points directly, limiting its usability. Song [28] used the LRC method to study the equivalent static wind loads of dome structures. The study mainly investigated the structural response when the first modal frequency is 0.5354 (cycle/sec), finding that the LRC method's results closely resembled time history solutions, making it a suitable, time-saving approach for designing large-span dome structures primarily guided by background response.

Equivalent static wind load methods have long been one of the main topics in wind engineering academia. The primary reason is that only some approaches are suitable for some types of structural load systems. As the wind-induced response arises from the relative proportion of background and resonant responses, attention must be paid not only to the approaching flow characteristics of the wind force but also to the interplay between wind forces and structural behavior, which is of paramount importance. The equivalent static wind load methods specified in the regulations are mainly restricted to structural systems that tend towards the characteristics of tall buildings. That is, the related structural modes in the "Gust Response Loading Factor Method" that is employed must be very pronounced and separated. As a result, it can be anticipated that structures with less distinct characteristics and high spatial correlation, such as low-rise building structures or large-span roof structures, are highly likely to experience distortion in design load. Internationally, many scholars in wind engineering and structural design have reached a consensus on the issue of equivalent static wind loads. No specific set of equivalent design wind load theories applies to all structural systems. Moreover, suppose the calculation of design wind loads considers the perspective of the initial design. In that case, care must be taken to avoid creating an excessive number of load combinations, which could paradoxically lead to confusion for designers.

This paper intends to introduce the concept of the multiple-target equivalent static wind loads and to demonstrate how to reduce the heavy computational burden when the structural designer needs to consider multiple loading effects of the target structure. The wind tunnel test of an elliptical-shaped stadium structure with a flat roof is first conducted to show the fundamental aerodynamic characteristics. The methodologies of the background-component wind force based on the load-response-correlation (LRC) method and the resonant-component wind force based on the inertial force method are then introduced for the specification of single-target equivalent static wind loads. Finally, the clustering analysis technique is adopted to explain the concept of the multiple-target equal static wind loads [29]. A decay index is proposed to indicate how the clustering technique improves the specification of equivalent static wind loads.

2. Experimental Setting and Structural Information

The research adopted the Atmospheric Boundary Layer Wind Tunnel Laboratory No.1 at Tamkang University's Wind Engineering Research Center [30] for wind tunnel tests of a large-span roof structure model. The wind tunnel facility is classified as an open-circuit, suction-type wind tunnel, as shown in Fig. (**1**). The testing section of

the wind tunnel has a length of 12.0 meters, a width of 2.2 meters, and a height of 1.8 meters. The ceiling height of the wind tunnel is adjustable, with a maximum adjustment height of 0.3 meters. The wind tunnel's dynamic section employs a centrifugal fan driven by a direct current, step-less varying-speed motor with a power capacity of 250 horsepower. Wind speed can be adjusted by controlling the rotational speed of the fan, and under normal operation, the wind speed ranges from 1.0 m/s to 28 m/s. The contraction ratio of the wind tunnel's inlet section is 3.6:1. At the front of the inlet section, honeycomb tubes and three layers of damping nets are installed, reducing the free-stream turbulence intensity within the wind tunnel to a range of 0.5% to 1%. Additionally, in the testing section near the dynamic section, there is a rotating working turntable with a diameter of 2 meters. The turntable can be controlled via a computer to rotate, and its angular measurement precision reaches ±0.5° as assessed by a digital angle meter. On the exterior of the wind tunnel, there is an observation room where experimental personnel can monitor the progress of the experiments through reinforced glass windows.

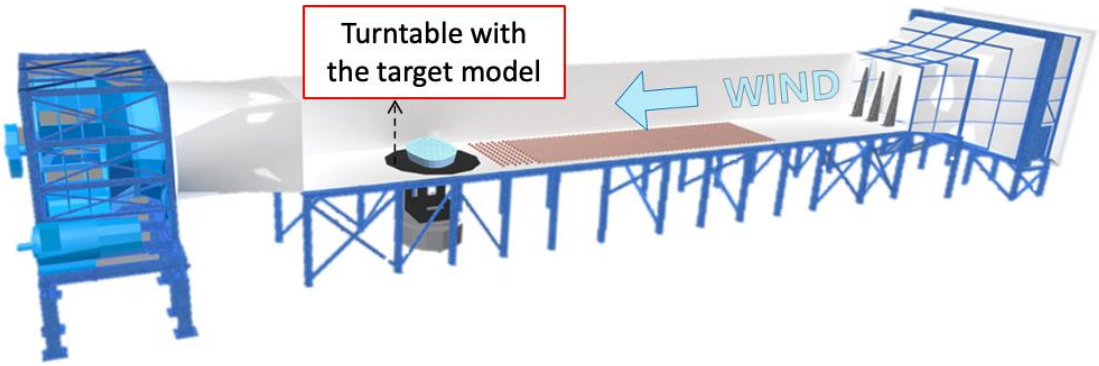

Figure 1: Wind tunnel facility at Tamkang University.

In this study, turbulence generators, such as spires and roughness elements, were positioned within the testing section, as depicted in Fig. (**2**), to simulate the flow field of a suburban atmospheric boundary layer [31]. A Cobra anemometer was utilized to measure the characteristics of the simulated wind field. In this experiment, the sampling frequency of the Cobra anemometer was set at 1000 Hz, with a sampling length of 60 seconds for each record, resulting in a total sampling length comprising 60,000 data points. Measurements were made progressively upwards from near the wind tunnel floor, yielding wind speed measurement records at 34 different heights. Fig. (**3**) shows the mean wind speed profile (left), turbulence intensity profile (center), and turbulence length integral scale diagram (right). Within Fig. (**3**) (left), the red line represents the theoretical wind speed profile where the terrain roughness index α is 0.25 [32]. The blue dots correspond to the experimentally measured average wind speed profile. The remarkable alignment between these lines demonstrates that the flow field meets the required criteria.

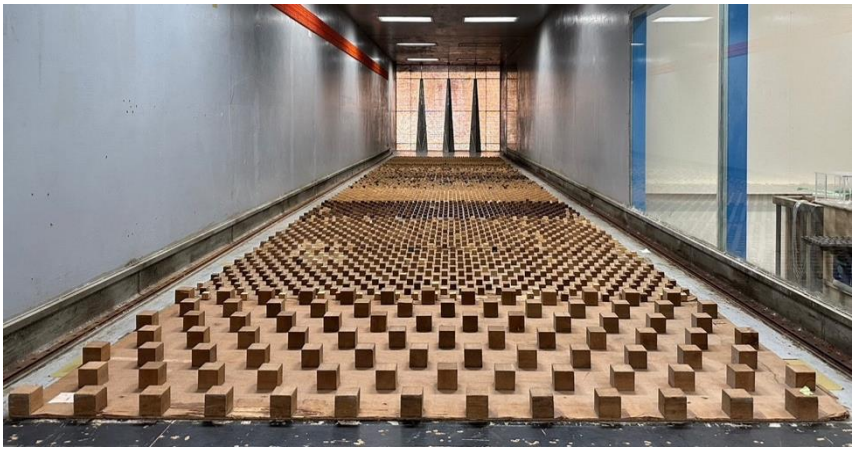

Figure 2: Photo of experimental setting within the wind tunnel.

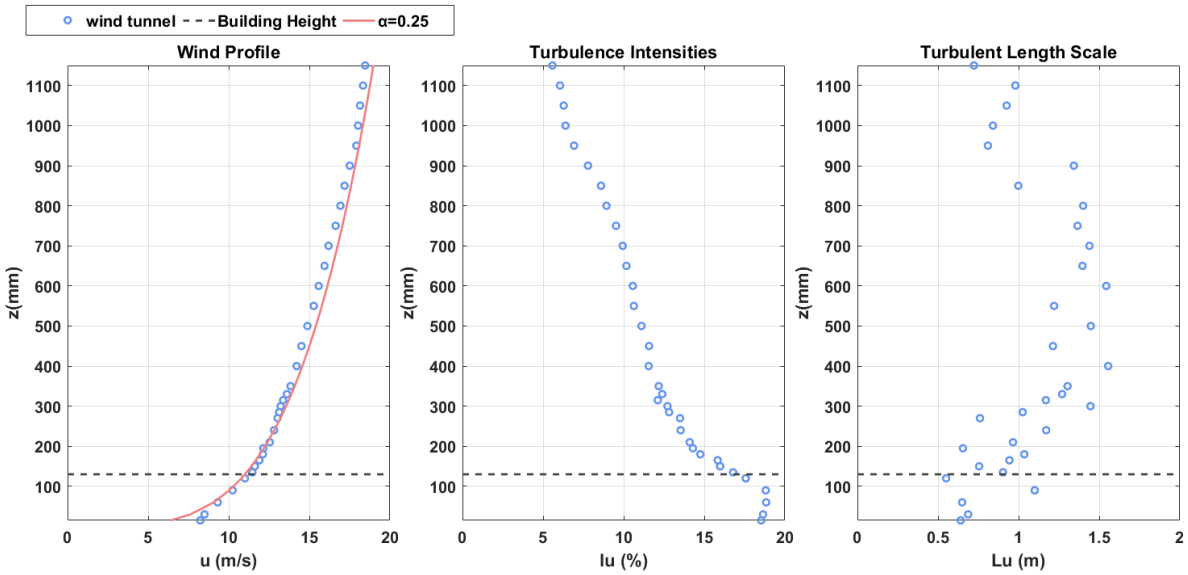

Figure 3: Flow characteristics of simulated suburban terrain.

Wind pressure measurement experiments were conducted using a scale model of a large-span sports arena. The model's dimensions were 56.6 centimeters in length, 46.4 centimeters in width, and 13 centimeters in height. The model was fabricated using 3D printing, and it included wind pressure taps — 192 on the side walls and 159 on the top surface, making a total of 351 taps. The wind pressure measurements were taken using PVC wind pressure tubing with a length of 90 centimeters [33]. The wind pressure model is illustrated in Fig. (**4**). The building's length scale was set at 1/250, correlating to the actual building dimensions of 141.5 meters in length, 116 meters in width, and 32.5 meters in height. To compute the wind speed at the height of the building, the basic design wind speed was set at 32.5 m/s, and the design wind speed at the actual building's height was then calculated. The wind speed at the height of the wind tunnel model was 11.5 m/s, leading to a velocity scale of approximately 1/2.5 and a time scale of 1/100. In other words, one second of measurement in the laboratory was equivalent to 100 seconds in the actual measurement [34]. The detailed experimental parameters are presented in Table **1**.

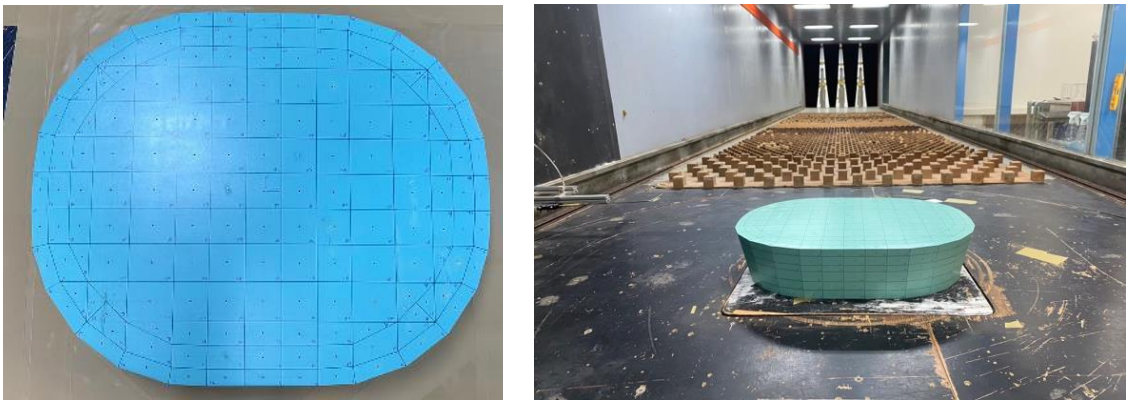

Figure 4: The scale model in this study (left) and its installation within the wind tunnel.

In conducting structural analysis, the finite element model primarily utilized beam elements to provide stiffness, while shell elements were employed to impart structural mass [35]. To simplify subsequent discussions, the cross-sectional dimensions of all beam and shell elements were assumed to be identical. The details of the element parameters are presented in Table **2**. The nodes of the finite element model were divided into four parts: 164 in the outer layer of the top surface, 132 in the inner layer of the top surface, 192 in the outer layer of the side

walls, and 160 in the inner layer of the side walls, totaling 648 nodes. Correspondingly, the beam elements are also divided into four parts: 391 in the outer layer of the top surface, 642 in the inner layer of the top surface, 352 in the outer layer of the side walls, and 448 in the inner layer of the side walls, amounting to 1833 in total. The shell elements are divided into 159 on the top surface and 192 on the side walls, making a total of 351. Fig. (**5**) shows the finite element model.

Table 1: Experimental parameters for wind pressure measurements.

	Scaled Model	Prototype	Scale
Depth	56.6 cm	141.5 m	1/250
Width	46.4 cm	116.0 m	
Height	13.0 cm	32.5 m	
Velocity at top	11.5 m/s	28.9 m/s	1/2.5
Sampling rate	500 Hz	5 Hz	1/100
Sampling time	600 s	16.7 s	
Testing angle	0°, 15°, 30°, 45°, 60°, 75°, 90°		

Table 2: Parameters for the finite element model.

Young's modulus for all beam elements	2.09×10^{11} N/m^2
Young's modulus for all shell elements	1.00×10^{-6} N/m^2
Weight density of shell elements	2.35×10^{4} N/m^3
Diameter of beam elements	0.10 m for top surfaces 0.35 m for side walls
Thickness of shell elements	0.12 m for top surfaces 0.35 m for side walls
Constraint condition	Fixed end at ground
Identified number of mode shapes	324

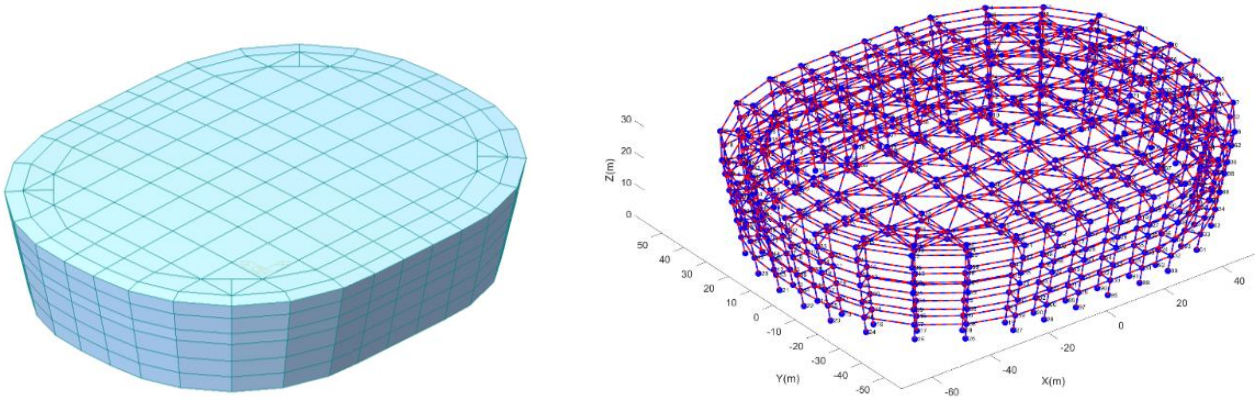

Figure 5: Diagram of the finite element model coded by MATLAB (left: shell, right: beam).

3. Aerodynamic Characteristics of Wind Loads

Upon completion of the instantaneous wind pressure measurements of the scale model, the obtained surface wind pressures were normalized by subtracting the mean static pressure measured on the Pitot tube erected at

the model's height and then divided by the mean wind pressure at the model's height to obtain the instantaneous wind pressure coefficients. As the experimental study utilized a sufficiently long sampling time, the wind pressure measurement data for each wind attack angle could be divided into 100 segments according to an actual field duration of ten minutes. Considering the premise of data stability, the mean and fluctuating values of 100 segments of instantaneous wind pressure coefficients could be ensemble-averaged and plotted into contour distribution maps for observing the fundamental aerodynamic characteristics. Fig. (**6**) illustrates the contour distribution maps of the mean and fluctuating wind pressure coefficients on the model's surfaces. Due to space constraints, Fig. (**6**) only displays the results at 0°, 45°, and 90°. The roof surface exhibited negative pressures, particularly at the windward edges. With the change in wind direction, the maximum negative and positive pressure exerted on the side walls simultaneously shifted to corresponding regions [36-38].

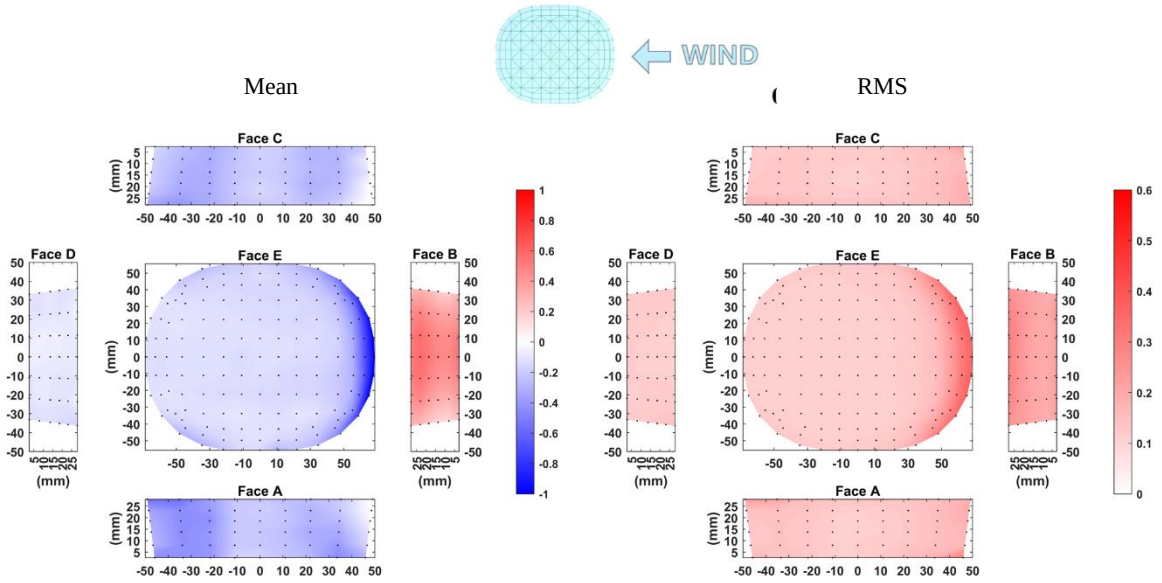

(a) Wind attack angle = 0°

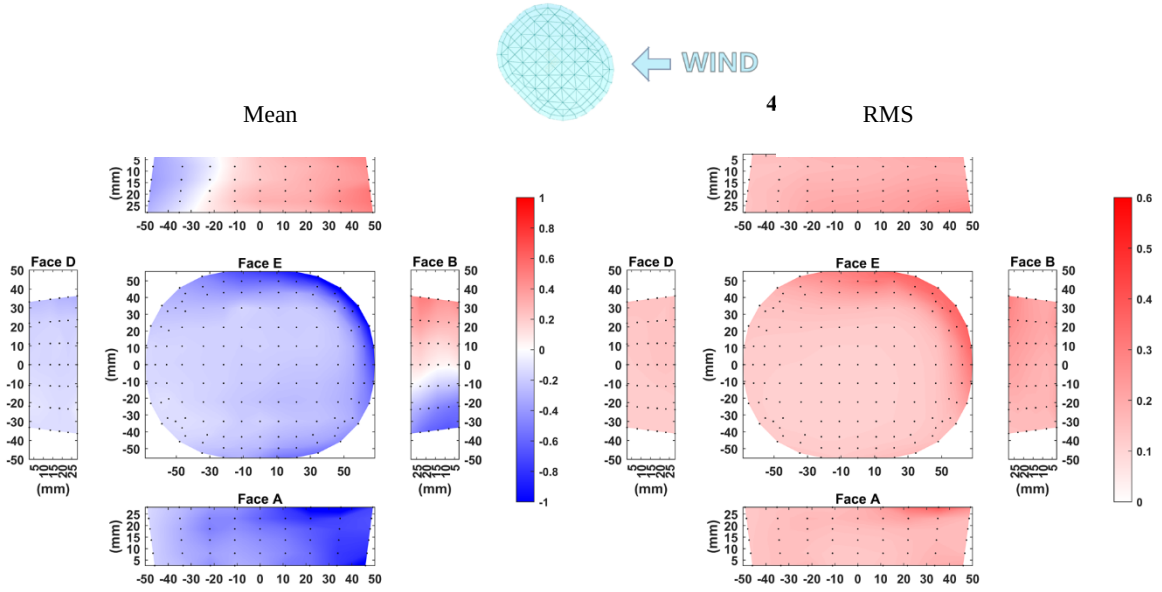

(b) Wind attack angle = 45°

(Figure 6) contd....

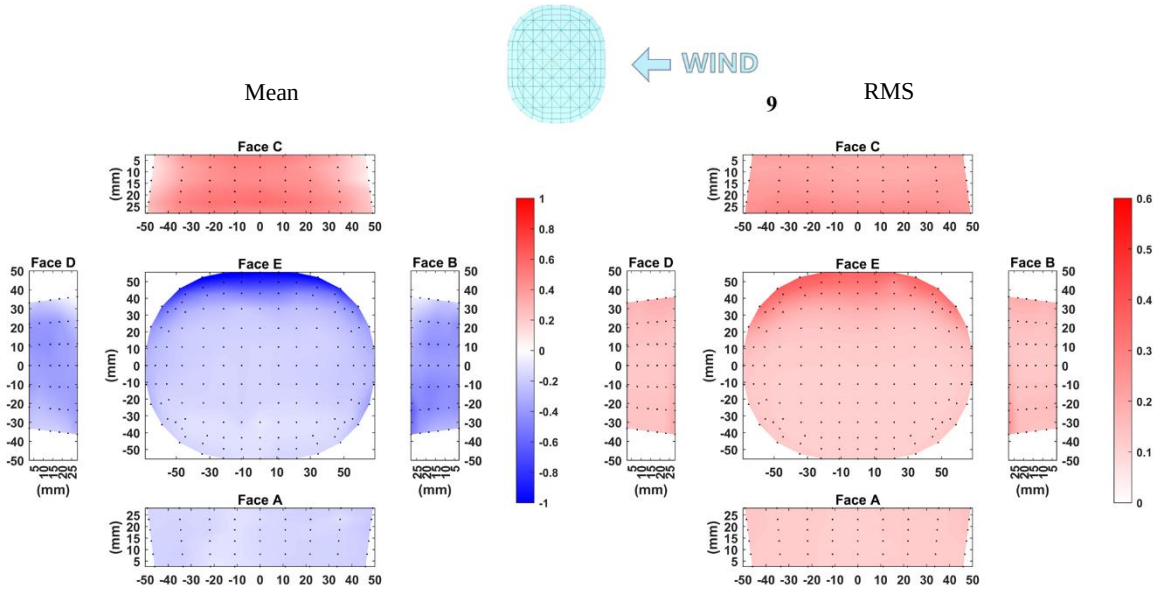

(c) Wind attack angle = 90°

Figure 6: Mean and fluctuating pressure coefficients.

4. Estimation of Single-Target Equivalent Static Wind Loads

In structural dynamic analysis, equivalent static loads can be deduced through the structural stiffness to represent the dynamic amplification effects caused by the background and the resonant wind forces [23]. These equivalent static loads are not actual external forces; instead, they are derived in different forms of equivalent static load distribution based on various design objectives and load effects. Therefore, it is necessary to consider load combinations. The response spectrum of some specific load effect can be divided into two parts: the spectral area caused by the background wind force and the spectral area instigated by the resonance effects of the structural mechanical transfer functions. Among them, the Load-Response-Correlation Method, abbreviated as the LRC method [18, 19], can be used to estimate the equivalent static loads of dynamic effects caused by the background wind force. Conversely, the inertia force method can be applied to estimate the equivalent static loads due to resonance effects [16, 23]. The following sections introduce the LRC method, the inertia force method, and how to combine the background and the resonant wind forces into an equivalent static wind load for some target load effects.

4.1. The LRC Method for the Background Wind Force

The Load-Response-Correlation (LRC) method, proposed by Kasperski and Niemann in 1992 [18], applies to various structural entities for estimating structural responses under the influence of external forces. This method employs the correlation between structural responses and externally applied loads to estimate design loads, where the form of the load effect is related to the influence function of the structure itself. The extreme load effect can be expressed as

$$r_{max} = \bar{r} + g_B \times \sigma_B \tag{1}$$

$\bar{r}$ is the mean load effect. g_B is the peak factor for the background load effect. σ_B is the standard deviation of the background load effect caused by dynamic external loadings. Generally, the background peak factor g_B is usually assumed to be 3.5 - 3.7 [32]. In this study, we simply assumed g_B to be estimated as the peak factor of the approaching winds [39]. The mean load effect is expressed as

$$\bar{r} = [A] \times \{\bar{F}\} = \sum_{k=1}^{m} a_{ik} \times \bar{F}_k \tag{2}$$

In Equation (2), $\bar{r}$ is a $(n, 1)$ vector representing the mean load effect. $[A]$ is an influence coefficient matrix with (n, m) dimensions of some specific load effect. $\{\bar{F}\}$ is a $(m, 1)$ vector representing the mean wind load. n is the number of concerned elements, and m is the number of loading positions where the unit force is exerted. a_{ik} represents the load effect of the i-th member due to the unit force exerting on the k-th position.

The co-variance between the load effect and the dynamic loadings can then be expressed as Equation (3), where $[\sigma_{rF}^2]$ is a (n, m) matrix standing for the co-variance between the load effect and the loading. $[\sigma_F^2]$ is a (m, m) matrix representing the co-variance between loadings at different positions. Therefore, the co-variance $[\sigma_r^2]$ between load effects of different concerned elements can be derived in Equation (4), where $[A]^T$ is the transpose of $[A]$.

$$[\sigma_{rF}^2] = [A] \times [\sigma_F^2] = \sum_{k=1}^{m} a_{ik} \times \sigma_{F_{kl}}^2 \tag{3}$$

$$[\sigma_r^2] = [A] \times [\sigma_F^2] \times [A]^T = \sum_{k=1}^{m} \sum_{l=1}^{m} a_{ik} \times a_{il} \times \sigma_{F_{kl}}^2 \tag{4}$$

Substitute Equations (2) and (4) into (1) and obtain Equation (5) as follows.

$$r_{i_{max}} = \sum_{k=1}^{m} a_{ik} \times \bar{F}_k + g_B \times \frac{\sum_{k=1}^{m} a_{ik} \times \sum_{l=1}^{m} a_{il} \times \sigma_{F_{kl}}^2}{\sigma_{ri}} \tag{5}$$

Since the correlation between the loading and the load effect can be expressed as Equation (6), Equation (5) can be further rewritten as Equation (7).

$$\sigma_{r_i F_k}^2 = \rho_{r_i F_k} \times \sigma_{ri} \times \sigma_{F_k} \tag{6}$$

$$\begin{aligned} r_{i_{max}} &= \sum_{k=1}^{m} a_{ik} \times \bar{F}_k + g_B \times \sum_{l=1}^{m} a_{ik} \times \rho_{riFk} \times \sigma_{F_k} \\ &= \sum_{k=1}^{m} a_{ik} \times [\bar{F}_k + g_b \times \rho_{riFk} \times \sigma_{F_k}] \end{aligned} \tag{7}$$

The equivalent static wind load estimated by the LRC method is the combination of the mean load effect and the dynamic load effect (only the background part). In Equation (7), $r_{i_{max}}$ is the extreme (or maximum/minimum) load effect of the i-th concerned member, while $[\bar{F}_k + g_b \times \rho_{riFk} \times \sigma_{F_k}]$ is the equivalent static wind load.

4.2. The Inertia Method for the Resonant Wind Force

The inertial force method is a method for estimating the equivalent static wind loads for various modes of vibration, and it typically requires consideration of multiple modes to obtain results that approximate reality [39]. When a structure is subjected to wind forces, a resonant response occurs if the frequency of the external force coincides with the structure's effective frequency [40, 41]. Generally speaking, low-frequency modes contribute more noticeably to the resonant part than high-frequency modes. The following describes the method of calculating inertial forces.

Based on random vibration theory [42], the relationship between the displacement response spectrum and the force spectrum is written as Equation (8).

$$S_{x,m} = \frac{\sum_{i=1}^{N} \sum_{j=1}^{N} \phi_{im} \phi_{jm} S_{F,ij}^{C}}{16\pi^4 {n_m}^4 M_m^2 \left\{ \left[1 - \left(\frac{n}{\bar{n}_m} \right)^2 \right]^2 + \left[2\xi_m \left(\frac{n}{\bar{n}_m} \right) \right]^2 \right\}} \tag{8}$$

In the above equation, $S_{x,m}$ represents the displacement response spectrum of the m-th mode, $S_{F,ij}^{C}$ represents the co-spectrum of wind forces acting at the i-th node and the j-th node, $\tilde{n}_m$ is the effective frequency of the m-th mode, n_m is the structural frequency of the m-th mode, ϕ_m is the shape function of the m-th mode, ξ_m is the damping ratio of the m-th mode, N is the number of nodes, and M_m is the generalized mass of the m-th mode. The variance of the displacement response is estimated by integrating Equation (8). However, if the resonant wind force is simplified as a white-nose signal and all the corresponding frequencies can be considered independent individually, the integral of the mechanical function of the m-th mode can be simplified as follows.

$$\int |H(n)|^2 dn = \frac{1}{2}|H(n)|^2 = \frac{\pi}{2KC} = \frac{1}{4\xi^2 K^2} \times \pi\xi n = \frac{\pi n}{4\xi K^2} \tag{9}$$

K is the generalized stiffness and C is the generalized damping. Equation (8) is then rewritten as Equation (10).

$$\sigma_{r,m}^2 = \frac{\sum_{i=1}^{N}\sum_{j=1}^{N} \phi_{im}\phi_{jm} S_{ij}^{C}(n_m)}{64\xi_m \pi^3 {n_m}^3 M_m^2} \tag{10}$$

The inertia force method estimates the resonant load effect from the above derivations [16]. Therefore, the application of this method is to add the outcome of Equation (10) to the left-hand side of Equation (7) to include the resonant part to the extreme load effect. By the influence coefficient matrix of some specific load effect (not necessarily the displacement response), the equivalent static wind load is obtained. The following section explains the combination concept briefly.

4.3. Equivalent Static wind Load for Single-Target Load Effect

This study posits that the direction of the extreme response leads to the distinction between positive and negative signs in the extreme values. Therefore, in determining the extreme value of the structural response, if the mean structural response is positive, the extreme response of that structural member is taken as the positive maximum; if the mean structural response is negative, the extreme response of that member is taken as the negative maximum, and its absolute value is used. The single-target equivalent static wind load is reconstituted from the contributions made by the resonant and background load parts to the maximum value of a specific load effect. By determining the contribution weight factors based on the magnitude of the extreme response caused by the equivalent static wind loads of each part and various modes, they are then redistributed and combined into a set of specific dynamic extreme equivalent static wind loads [43]. Equation (11) is given to show the reconstitution of all parts.

$$r_{max} = \bar{r} + \sqrt{\hat{r}_B^2 + \hat{r}_R^2} \tag{11}$$

Considering the high similarity among multiple structural modes of the large-span roof structures, Equation (11) is usually changed to Equation (12).

$$r_{max} = \bar{r} + \sqrt{\left(g_B \sigma_{r,B}\right)^2 + {g_R}^2 \sum_{m=1}^{Q} \sigma_{r,R_m}^2} \tag{12}$$

where

$$g_R = \sqrt{2\,ln(\nu T)} + \frac{0.577}{\sqrt{2\,ln(\nu T)}} \tag{13}$$

ν is the structural frequency of the first mode, and T is the loading time of wind force (in this study, 10 minutes). $\sum_{m=1}^{Q} \sigma_{r,R_m}^2$ indicates the resonant load effect is estimated by the first Q modes.

Because the load effect calculated using the LRC method pertains to the internal forces within the concerned members, and the resonant response relates to displacement reactions, it is necessary to utilize different influence coefficient matrices of different load effects. This allows for the conversion of displacement response variance into the variance of the internal force structural response, aligning it with the internal force structural response calculated by the LRC method. By employing Equation (12), the mean, background, and resonant load effects can be combined to yield the single-target equivalent static wind load.

4.4. Validation of Single-Target Equivalent Static Wind Loads

To save space, the assessment of the single-target equivalent static wind load on the large-span roof model employed in this research is limited in scope. Accordingly, the verification process focuses solely on the axial forces within the beam members of the roof's inner and outer layers. As depicted in Fig. (**7**), the designated beam positions of interest are highlighted by the red lines. The exterior layer's members are assigned numbers ranging from 1 to 322, while the interior layer's members are numbered from 323 to 580.

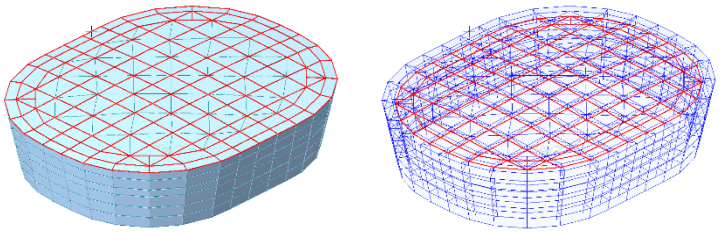

(a) Exterior surface **b) Interior surface**

Figure 7: Observed beam members of the employed model in this study.

Fig. (**8**) illustrates the extreme axial force results for two groups of beam members at a wind attack angle of 0 degrees, obtained through the time-domain dynamic analysis and the equivalent static analysis incorporating only the mean and background responses. In the figure, the red line represents the true solution derived from time

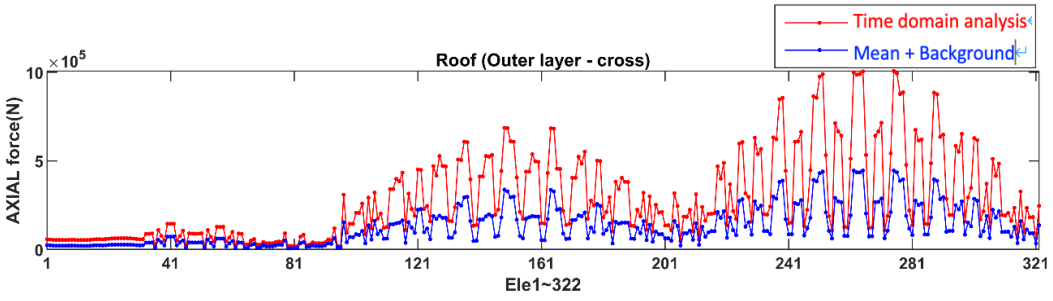

(a) Beam members of the exterior surface

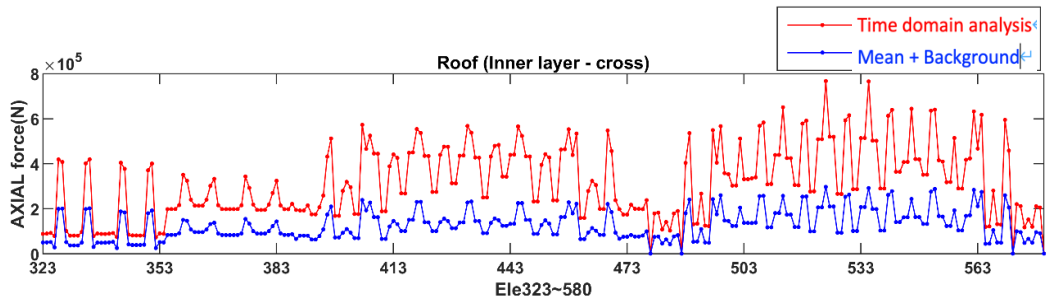

(b) Beam members of the interior surface

Figure 8: Extreme axial forces of observed beam members based on the LRC method.

domain dynamic analysis, while the blue line represents the predicted results of the mean and background responses obtained through the LRC method. The figure shows that although the predicted results exhibit a similar trend to the true solution, they are consistently lower than the true solution. This indicates that when considering only the mean and background responses, the predicted results are generally underestimated, highlighting the significance of resonant responses. Fig. (**9**) shows the verification results of the LRC method.

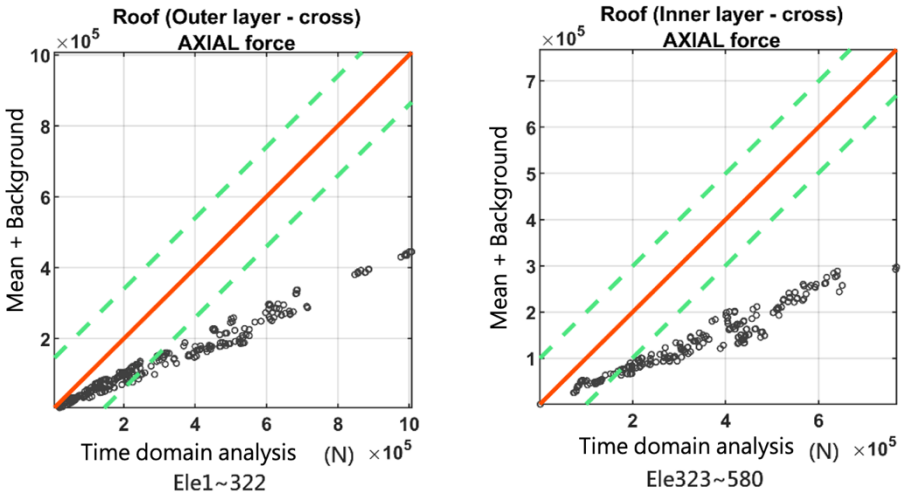

(a) Exterior surface **(b) Interior surface**

Figure 9: Verified axial force results of the LRC method.

Fig. (**10**) illustrates the extreme axial force results for the same two groups of beam members at a wind attack angle of 0 degrees incorporating the mean, background, and resonant responses. In the figure, the added brown line represents the predicted results of the mean, background, and resonant responses obtained through the LRC

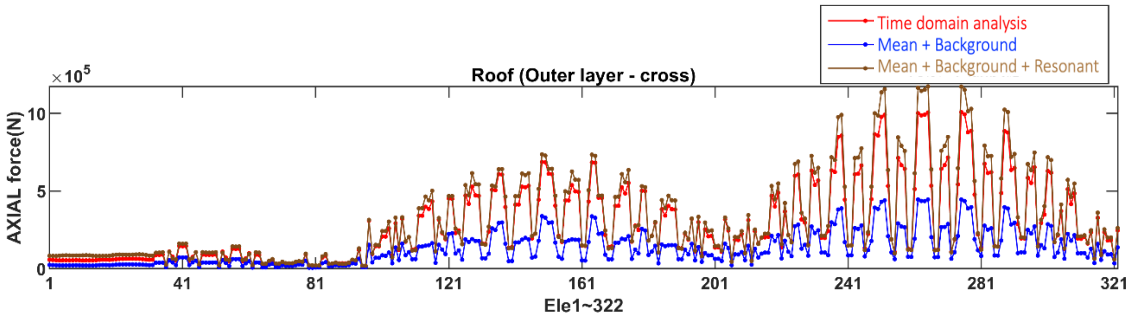

(a) Beam members of the exterior surface

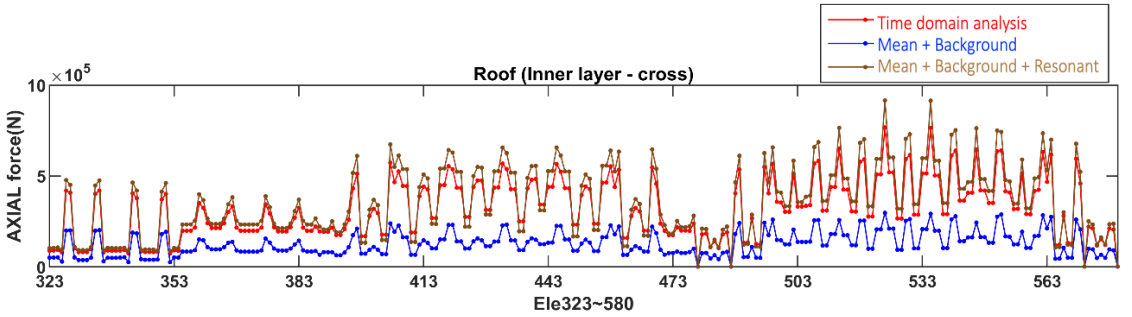

(b) Beam members of the interior surface

Figure 10: Extreme axial forces of observed beam members based on the LRC method & the inertia method.

method and the inertia method. The figure shows that, with the addition of the resonant part, the predicted results are much closer to the true solution and, in most cases, slightly larger than the true solution. This is usually acceptable since structural engineers tend to give a conservative design. In Fig. (**11**), the verification results are shown to be much improved. Here the resonant responses of the observed beam members are assumed to be reconstituted by the first 100 modes, which contribute more than 90% of energy among 324 modes. The slight conservativeness shown in Fig. (**10**-**11**) is supposed to be the assumption of the first mode resonant peak factor. The same verification results can be indicated in the internal moments of the same two groups of beam members in Fig. (**12**), which shows the generally satisfying predicted results based on the LRC method and the inertia method, i.e., the combination of the mean, background, and resonant results.

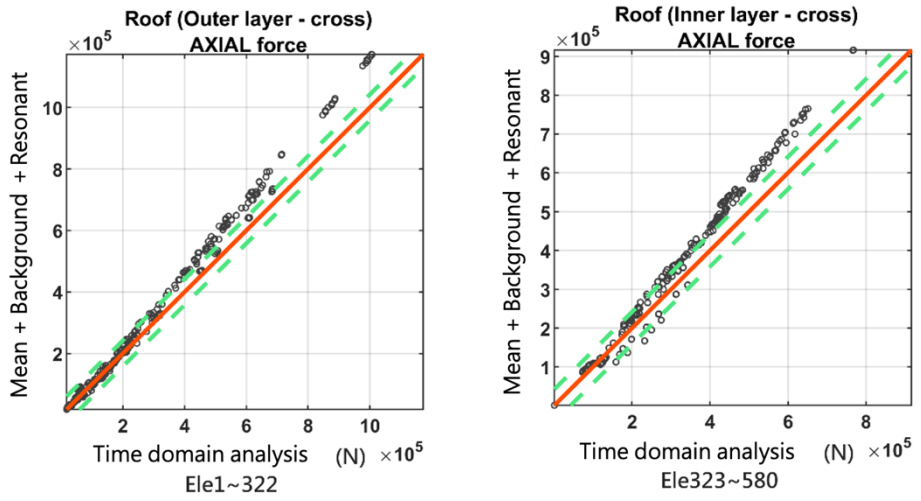

(a) Exterior surface **(b) Interior surface**

Figure 11: Verified axial force results of the LRC method and the inertia method.

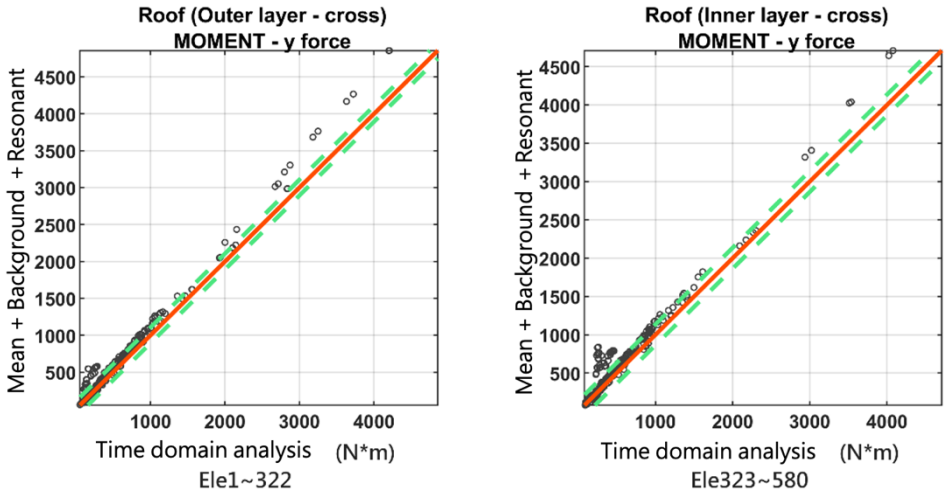

(a) Exterior surface **(b) Interior surface**

Figure 12: Verified internal moment results of the LRC method and the inertia method.

5. Specification of Multiple-Target Equivalent Static Wind Loads

Cluster analysis theory has been increasingly applied in recent years to information processing related to artificial intelligence [29, 44–46]. It effectively identifies central characteristics within clusters that possess certain attributes. As data volume increases or data characteristics become more complex, the utility of this method becomes more pronounced. Therefore, this study employs artificial intelligence-based clustering methods to

address the substantial number of combinations arising from the background and resonant wind forces in large-span roof structures. At the same time the approach preserves the predictive accuracy of the original wind field characteristics and structural responses.

5.1. Determination of Multiple-Target Equivalent Static Wind Loads

The K-means clustering method represents one of the fundamental techniques within the category of partitional clustering [47]. Its primary objective involves identifying representative data points, referred to as cluster centers, from a large dataset. These cluster centers are subsequently employed for tasks such as data compression or classification. Through data compression, a reduced number of data points are used to represent a substantial amount of data, thereby achieving data compression effects. On the other hand, data classification entails utilizing a limited set of representative points to characterize data belonging to specific categories. This not only diminishes data volume and computational demands but also mitigates the influence of noise on outcomes. When employing the K-means clustering method, it is imperative to specify the number of clusters. Subsequently, through iterative optimization, the method progressively minimizes the value of the error objective function until the final clustering outcome is achieved.

Huang and Lo [47] adopted the proper orthogonal decomposition (POD) method [48, 49] to decompose the fluctuating pressures over a specific surface into several orthogonal modes (POD modes). Since the POD modes constitute an orthogonal coordinate system, the single-target equivalent static wind load of some specific load effect can be projected onto these POD modes, assuming that all these POD modes are multiple-dimensional basic vectors. The projection can be expressed as Equation (14).

$$\{\hat{P}_M\} = \mathrm{c}_1\{\psi_{1\times M}\} + \mathrm{c}_2\{\psi_{2\times M}\} + \cdots = [\psi]\{C\} \tag{14}$$

In Equation (14), $\{\hat{P}_M\}$ represents the single-target equivalent static wind load. $[\psi]$ is the POD mode matrix. $\psi_{i\times M}$ is the i-th POD mode. M is the number of load positions where the equivalent static wind load is exerted. $\{C\}$ is the weighting coefficient vector that constitutes all the POD modes into the single-target equivalent static wind load. Due to the orthogonality of the POD modes, $\{C\}$ can be considered a vector in the linear subspace. Based on Equation (14), the determination of a multiple-target equivalent static wind load can be derived by first selecting the concerned load effects of multiple target members. Then, the weighting coefficient vectors of the associated equivalent static wind loads are found and assembled into a weighting coefficient matrix as in Equation (15).

$$Wc = \begin{bmatrix} c_{11} & \cdots & c_{1j} \\ \vdots & \ddots & \vdots \\ c_{k1} & \cdots & c_{kj} \end{bmatrix} \tag{15}$$

In Equation (15), there are k load effects of k members selected for one multiple-target equivalent static wind load. Thirdly, the weighting coefficient matrix can be clustered into groups by the K-mean method. Finally, the multiple-target equivalent static wind load of the c-th cluster originates from the linear combination of all single-target equivalent static wind loads in the c-th cluster. The realization of the c-th multiple-target equivalent static wind load is constructed by Equation (16).

$$R_{max} \approx R_s = \mathrm{A}^c_{c\times j} p^c_{j\times 1} \tag{16}$$

R_{max} is the assembly of the true load effects of selected members. R_s is the realization of the equivalent static response due to the multiple-target equivalent static wind load. $\mathrm{A}^c_{c\times j}$ is the associated influence function of the c-th cluster. $p^c_{j\times 1}$ is the load pattern of the multiple-target equivalent static wind load of the c-th cluster.

5.2. Efficiency of Clustering Analysis Technique for Various Kinds of Load Effects

The following examinations are divided into two parts: (1) multiple-target equivalent static wind load for individual load effects and (2) multiple-target equivalent static wind load for two kinds of load effects. In the first examination, extreme axial forces and extreme internal moments are separately approximated by clustering

analysis. In the second examination, extreme axial forces and extreme internal moments are mixed for cluster analysis. The first group, beam members of the exterior surface, in the previous section, is adopted for demonstration. Besides the extreme axial force, the internal moment is also included as the second kind of load effect.

Fig. (**13**-**14**) shows the comparisons of predicted axial force and internal moment results of the first examination for the beam members of the exterior surface. In all the subfigures, the horizontal axis stands for the predicted load effects based on single-target equivalent static wind loads. The vertical axis stands for the predicted load effects based on multiple-target equivalent static wind loads. Here we do not mix the axial load effects with the internal moment effects for the assembly of the weighting coefficient matrix and the clustering analysis. The two load effects are conducted individually to determine their own multiple-target equivalent static wind loads. The number of clusters for this group of beam members can range from 1 to 322. If the cluster number is 322, there will be 322 multiple-target equivalent static wind loads, the same as 322 single-target equivalent static wind loads. In Fig. (**13**) or (**14**), six subfigures show six ratios of cluster numbers to the maximum cluster number (322). As the cluster ratio increases, the differences between the single- and the multiple-target equivalent static wind loads decrease to perfectly 0 when the ratio is 1. It is supposed that when the ratio approaches some level, most members can be included in a satisfying range for the multiple-target equivalent static wind loads.

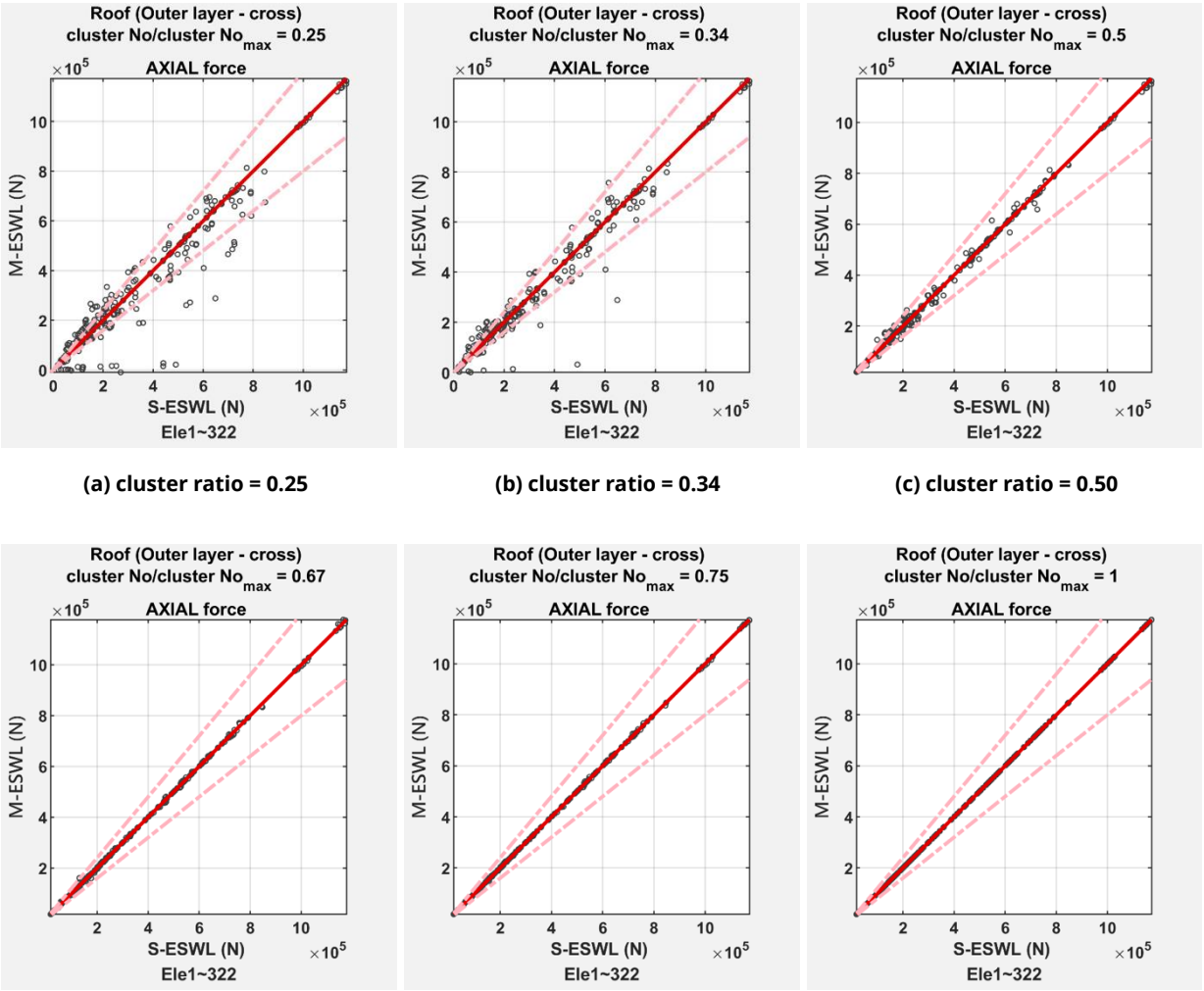

(a) cluster ratio = 0.25 **(b) cluster ratio = 0.34** **(c) cluster ratio = 0.50**

(d) cluster ratio = 0.67 **(e) cluster ratio = 0.75** **(f) cluster ratio = 1.00**

Figure 13: Comparisons of predicted axial force results based on multiple- and single-target equivalent static wind loads.

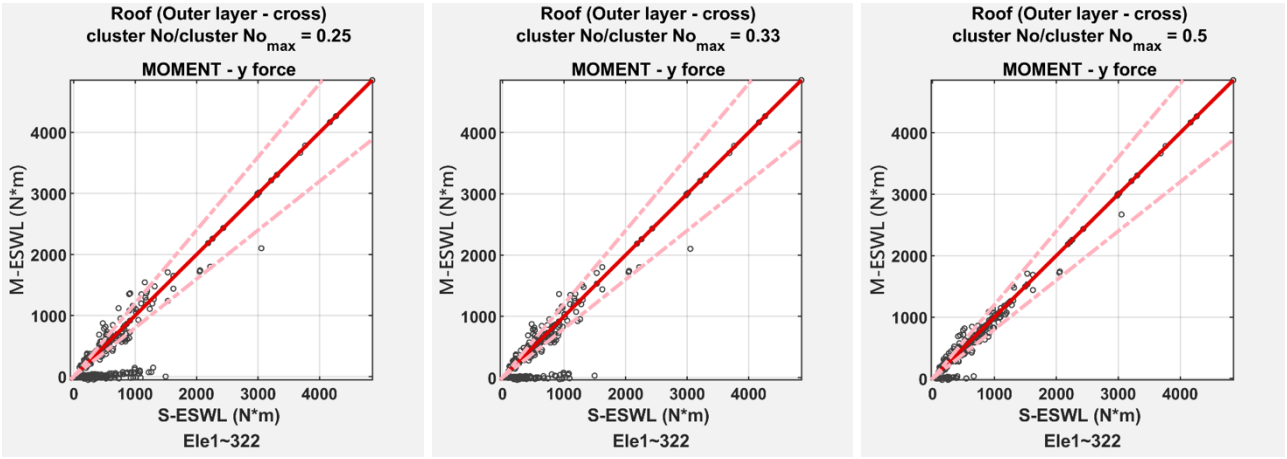

(a) cluster ratio = 0.25 **(b) cluster ratio = 0.34** **(c) cluster ratio = 0.50**

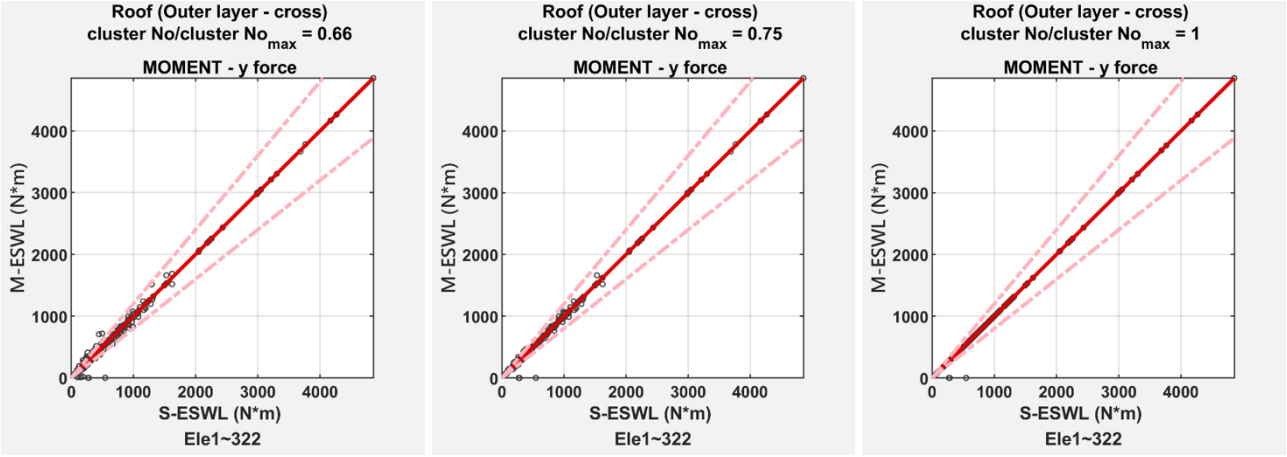

(d) cluster ratio = 0.67 **(e) cluster ratio = 0.75** **(f) cluster ratio = 1.00**

Figure 14: Comparisons of predicted internal moment results based on multiple- and single-target equivalent static wind loads.

To understand whether the clustering analysis technique is suitable for mixing various load effects, Fig. (**15**-**16**) are plotted in the same cluster ratios for the second examination. If comparing Fig. (**13**-**16**), it would be difficult to tell the slight differences made by mixing load effects. To effectively explain how the prediction becomes with the cluster ratio, the root-mean-square error (RMSE) value is estimated for each cluster ratio. Take the first subfigure in Fig. (**15a**) as an example, the RMSE value for the cluster ratio = 0.25 is calculated by Equation (17).

$$\mathrm{RMSE}^{*} = \sqrt{\frac{1}{n}\sum_{i=1}^{n}\left(X_{1,i} - X_{2,i}\right)^{2}} \tag{17}$$

$X_{1,i}$ is the i-th predicted load effect by the multiple-target equivalent static wind load, $X_{2,i}$ is the i-th predicted load effect by the single-target equivalent static wind load, n is the total number of concerned members. When the cluster ratio is 1, i.e., the cluster number equals the total number of the single-target equivalent static wind loads, RMSE^{*} is labeled as $\mathrm{RMSE}_{\max}{}^{*}$. An exponential decay function is proposed to represent how the RMSE ratio decreases with the cluster ratio increases as follows.

$$\begin{gathered} y = \mathrm{e}^{-kx} \\ y = \mathrm{RMSE}^{*}/\mathrm{RMSE}_{\max}{}^{*} \\ x = cluster\_no/cluster\_no_{max} \end{gathered} \tag{18}$$

In Equation (18), k is the decay index that shows how efficiently the cluster analysis reduces the number of equivalent static wind loads.

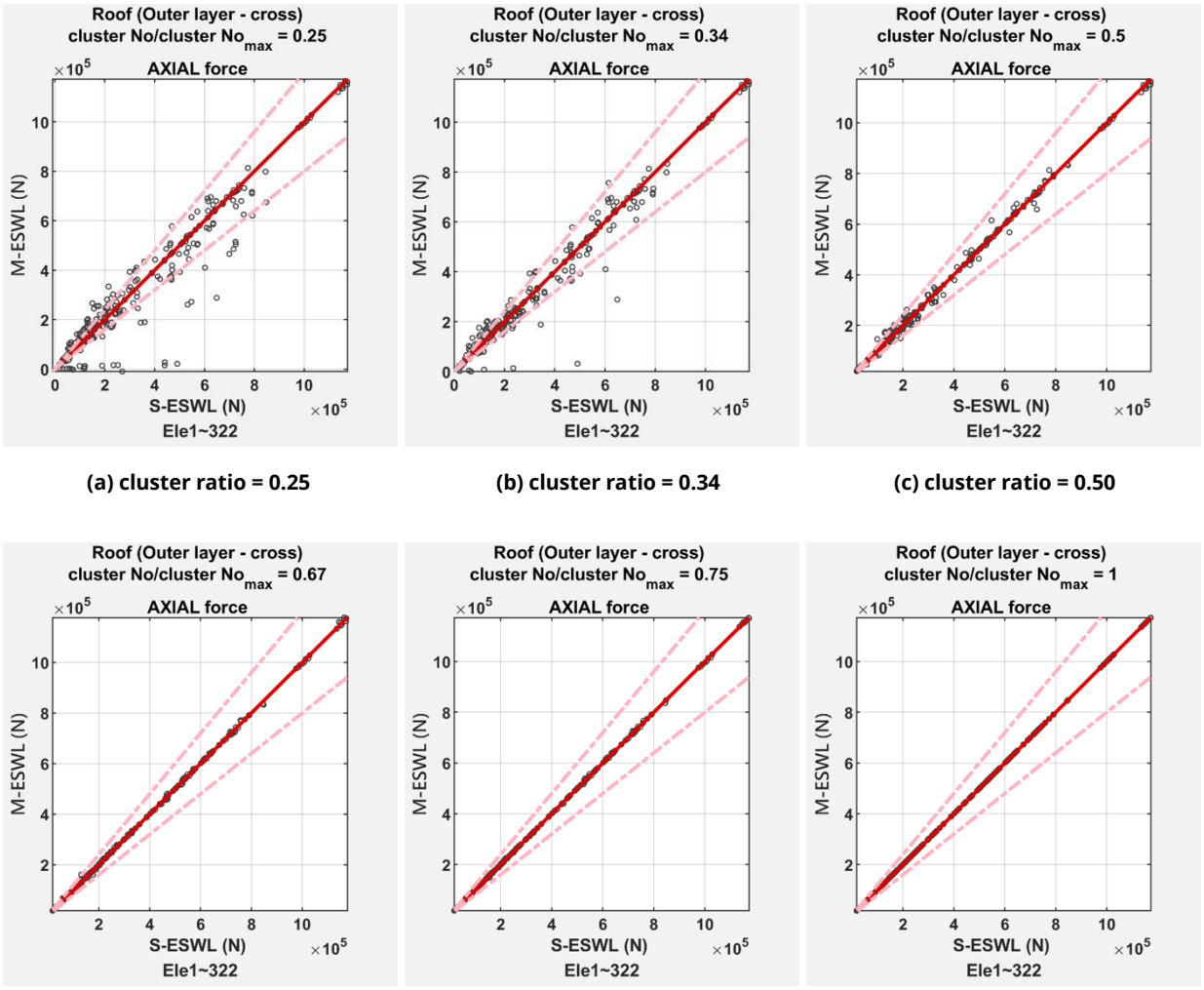

(a) cluster ratio = 0.25 **(b) cluster ratio = 0.34** **(c) cluster ratio = 0.50**

(d) cluster ratio = 0.67 **(e) cluster ratio = 0.75** **(f) cluster ratio = 1.00**

Figure 15: Comparisons of predicted axial force results based on multiple- and single-target equivalent static wind loads (two load effects are mixed for clustering).

Fig. (**17** -**18**) shows the fitting results of the RMSE ratios by Equation (18). The relationships between the estimated RMSE ratios and the cluster ratios indicate that, with the mixed load effects, i.e., the clustering conducted by mixing the axial forces and the internal moments of the beam members of the exterior surface show a faster-decaying tendency than the individual cluster analysis. This is supposed to be the high similarity between the behaviors of the axial forces and the internal moments when the beam members are excited by the same wind loads. Generally speaking, although not perfectly correlated, the highly correlated two load effects have enhanced the weighting of some specific single-target equivalent static wind loads. In Fig. (**17a**), the decay index is 4.844, slightly less than 5.997 in Fig. (**17b**). Fig. (**18**) follows the same tendency.

In another viewpoint of judging whether the beam members are predicted with good extreme load effects or not, we can select a threshold error percentage for further explanation of mixed clustering analysis. For example, if we specify 20% is the error difference threshold percentage between the individual clustering result and the multiple-clustering result, every time we attempt one cluster ratio, the number of those beam members whose difference errors are smaller than 20% are selected, and normalized by the total beam member number. As the cluster ratio increases, the number we select will also increase since the multiple-target equivalent static wind loads

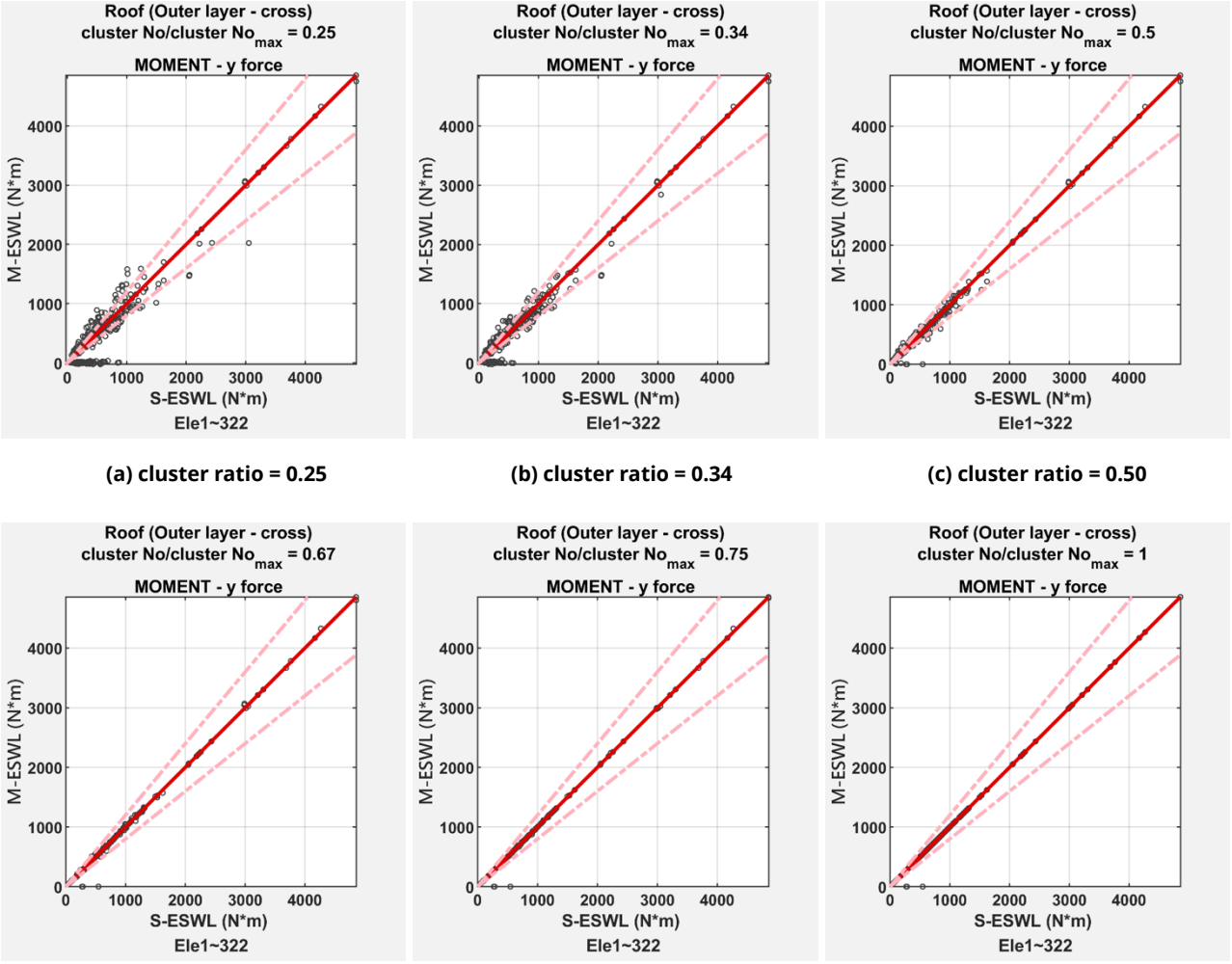

Figure 16: Comparisons of predicted internal moment results based on multiple- and single-target equivalent static wind loads (two load effects are mixed for clustering).

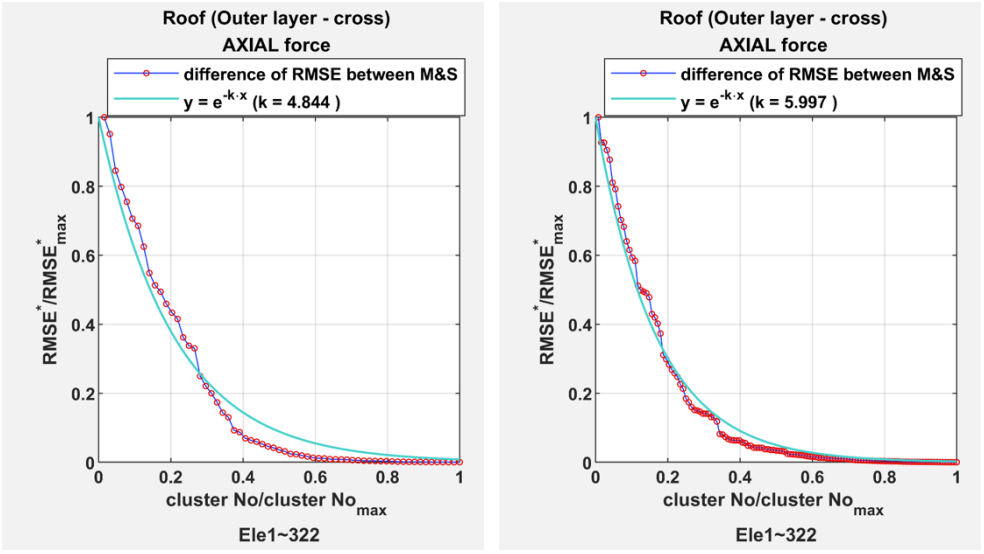

Figure 17: Fitting results of RMSE ratios for extreme axial forces due to individual and mixed clustering.

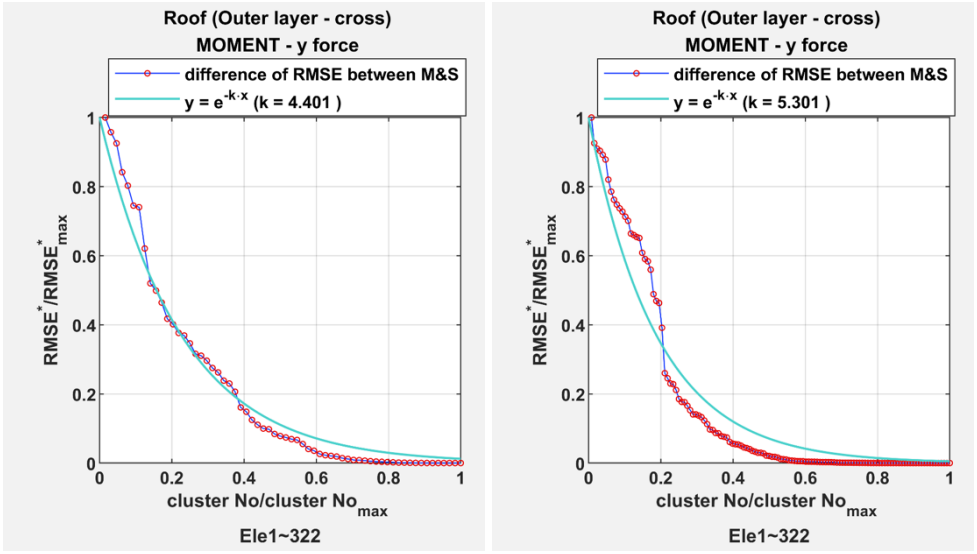

(a) Individual clustering **(b) Mixed clustering**

Figure 18: Fitting results of RMSE ratios for extreme internal moments due to individual and mixed clustering.

tend to act like single-target equivalent wind loads. In Fig. (**19**), the horizontal axis represents the cluster ratio, and the vertical axis represents the non-exceedance probability of the beam members whose difference errors are smaller than 20%. From both subfigures of axial forces and internal moments, the mixed clustering analyses show faster growth in approaching 100% non-exceedance probability, which explains the same conclusion as Fig. (**17**-**18**).

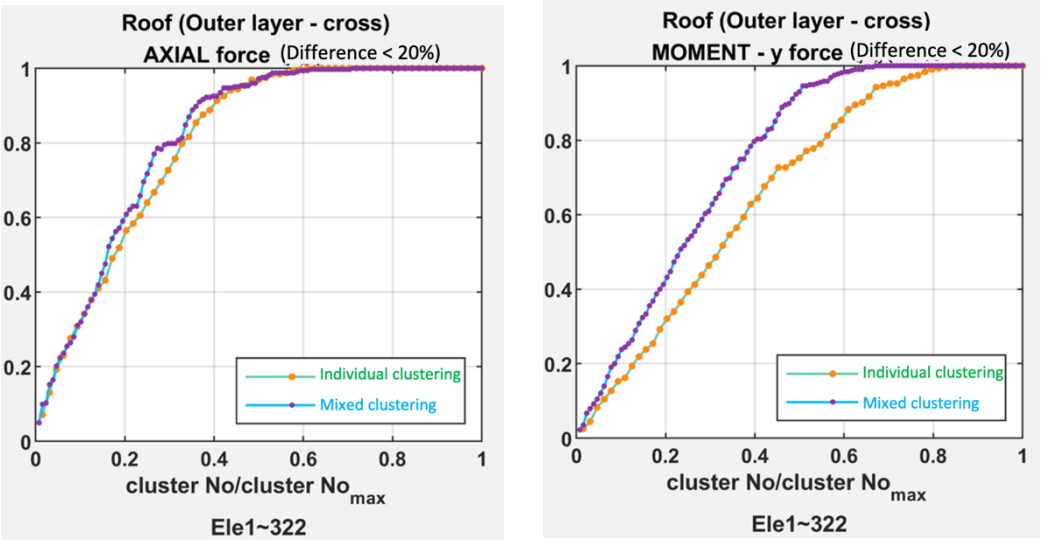

(a) Axial forces **(b) Internal moments**

Figure 19: Non-exceedance covering probability distributions of load effect differences less than 20%.

6. Conclusions

In this study, the commonly known equivalent static wind load for a single-target load effect was briefly introduced. The background wind force estimated by the LRC method and the resonant wind force estimated by the inertia method were explained and validated with the wind tunnel test results and the idealized finite element model of a large-span roof structure model. In the example given in this paper, the resonant response was found to be very dominant. Clustering analysis was then applied to group several single-target equivalent static wind loads for a multiple-target equivalent static wind load. If the cluster number is assumed to be as many as the

number of single-target equivalent static wind loads for all the concerned load effects of structural members, the clustering analysis made no difference to the prediction results. It proved no efficiency in reducing the number of load cases. On the other hand, if the cluster number was assumed not sufficient, the prediction accuracy was poor to replace the single-target equivalent static wind loads.

An exponential form with a decay index was proposed to find how effective the determination of the multiple-target equivalent static wind loads is. From the results of individual clustering and mixed clustering of two load effects, it was found that when the cluster ratio is larger than 0.3 – 0.4, i.e., reducing the number of the single-target equivalent static wind loads to about 30% – 40%, most predictions were found to be good. Further, when mixed clustering was applied to make clusters, the decay was even faster than the individual clustering. This is supposed to be the high similarity between the behaviors of the axial forces and the internal moments when the beam members are excited by the same wind loads.

Nevertheless, how to select the target load effects of some concerned structural members is always the key point to deciding how many equivalent static wind loads are necessary for structural analysis. Besides, the huge number of potential factors to alter the wind loads on the structures sometimes make it a difficult task to keep those effective load patterns for the subsequent combinations with the dead load and the live load. Although the example given in this study was idealized in its structural member choices, some factors are still necessarily taken into account, such as wind attack angles, different positions of the structural members, various load effects, and so on. All these potential factors intuitively determine multiple-target equivalent static wind loads even more difficult to generate. The authors believe that the artificial intelligence technique shall help deal with the complicated clustering analysis to identify some acceptable number of effective equivalent static wind loads.

Conflict of Interest

The authors declare that they have no known competing financial interests or personal relationships that could have appeared to influence the work reported in this paper.

Funding

This study is financially supported by the National Science and Technology Council research projects: MOST 111-2221-E-027-021.

Acknowledgments

The authors would like to thank the Wind Engineering Research Center at Tamkang University for providing technical support.

References

[1] Takahashi T. AIJ Recommendations for Loads on Buildings 2015. Architectural Institute of Japan; 2019.

[2] Eurocode 1: Actions on structures - Part 1-4: General actions - Wind actions (includes Amendment A1: 2010 + Corrigendum AC: 2010) English translation of DIN EN 1991-1-4:2010-12. DIN-Sprachendienst; 2010.

[3] Guide for the assessment of wind actions and effects on structures (CNR-DT 207/2008), Advisory Committee on technical recommendations for constructions. National Research Council of Italy; 2010.

[4] International Standard: Wind actions on structures (ISO 4354:2009). International Standard Organization; 2009.

[5] Minimum design loads for buildings and other structures (ASCE/SEI 7-22). Structural Engineering Institute, American Society of Civil Engineers; 2022.

[6] Davenport AG. Gust loading factors. J Struct Div. 1967; 93: 11-34. https://doi.org/10.1061/JSDEAG.0001692

[7] Davenport A. The representation of the dynamic effects of turbulent wind by equivalent static wind loads. Proceedings of International Engineering Symposium on Structural Steel, Chicago: 1993.

[8] Solari G. Gust buffeting I: Peak wind velocity and equivalent pressure. J Struct Eng. 1993; 119: 365-82. https://doi.org/10.1061/(ASCE)0733-9445(1993)119:2(365)

[9] Solari G. Gust buffeting II: Dynamic along-wind response. J Struct Eng. 1993; 119: 383-98. https://doi.org/10.1061/(ASCE)0733-9445(1993)119:2(383)

[10] Zhou Y, Gu M, Xiang H. Alongwind static equivalent wind loads and responses of tall buildings. Part I: Unfavorable distributions of static equivalent wind loads. J Wind Eng Ind Aerodyn. 1999; 79: 135-50. https://doi.org/10.1016/S0167-6105(97)00297-3

[11] Zhou Y, Gu M, Xiang H. Alongwind static equivalent wind loads and responses of tall buildings. Part II: Effects of mode shapes. J Wind Eng Ind Aerodyn. 1999; 79: 151-8. https://doi.org/10.1016/S0167-6105(97)00298-5

[12] Zhou Y, Kareem A, Gu M. Gust loading factors for design applications. Proceedings of the 10th ICWE, Copenhagen: 1999.

[13] Kareem A, Zhou Y. Gust loading factor—past, present and future. J Wind Eng Ind Aerodyn. 2003; 91: 1301-28. https://doi.org/10.1016/j.jweia.2003.09.003

[14] Chen X, Kareem A. Equivalent static wind loads for buffeting response of bridges. J Struct Eng. 2001; 127: 1467-75. https://doi.org/10.1061/(ASCE)0733-9445(2001)127:12(1467)

[15] Yang C. A preliminary investigation on the design wind loads of arched roofs. Master thesis (Chinese). Tamkang University , 2005.

[16] Lin Y, Wang B. Application of equivalent static wind loads on bridge design. Struct Eng. 2014; 29: 27-39.

[17] Lo YL, Wu CH. Estimation for equivalent static wind load of dome roof structures. Proceedings of the 16th East Asia-Pacific Conference on Structural Engineering and Construction, Brisbane: Springer; 2019, p. 415-26. https://doi.org/10.1007/978-981-15-8079-6_40

[18] Kasperski M, Niemann H-J. The L.R.C. (load-response-correlation) - method a general method of estimating unfavourable wind load distributions for linear and non-linear structural behaviour. J Wind Eng Ind Aerodyn. 1992; 43: 1753-63. https://doi.org/10.1016/0167-6105(92)90588-2

[19] Kasperski M. Extreme wind load distributions for linear and nonlinear design. Eng Struct. 1992; 14: 27-34. https://doi.org/10.1016/0141-0296(92)90005-B

[20] Wang Y. Application of LRC method on the equivalent static wind load of large span structures. Master thesis (Chinese). Tamkang University, 2011.

[21] Katsumura A, Tamura Y, Nakamura O. Universal wind load distribution simultaneously reproducing largest load effects in all subject members on large-span cantilevered roof. J Wind Eng Ind Aerodyn. 2007; 95: 1145-65. https://doi.org/10.1016/j.jweia.2007.01.020

[22] Holmes J. Optimized peak load distributions. J Wind Eng Ind Aerodyn. 1992; 41: 267-76.

[23] Holmes JD. Effective static load distributions in wind engineering. J Wind Eng Ind Aerodyn. 2002; 90: 91–109. https://doi.org/10.1016/S0167-6105(01)00164-7

[24] Hongo T. Experimental studies of fluctuating wind pressures on dome-like roofs. PhD thesis (Japanese). Wind Engineers, JAWE, 1995, (62): p. 23-33. https://doi.org/10.5359/jawe.1995.23

[25] Uematsu Y, Yamada M, Inoue A, Hongo T. Wind loads and wind-induced dynamic behavior of a single-layer latticed dome. J Wind Eng Ind Aerodyn 1997; 66: 227–48. https://doi.org/10.1016/S0167-6105(97)00133-5

[26] Holmes J. Equivalent static load distributions for resonant dynamic response of bridges. Proceedings of the 10th International Conference on Wind Engineering, Copenhagen: 1999.

[27] Davenport A. Missing links in wind engineering. Proceedings of the 10th ICWE, Copenhagen: 1999.

[28] Song J. Optimized equivalent static wind load of large-span-roof structures based on cluster analysis technique. Master thesis (Chinese). National Taipei University of Technology; 2022.

[29] Huang MH, Lo YL. A refined method of multi-target equivalent static wind loads: A bridge case. J Wind Eng Ind Aerodyn. 2021; 212: 104609. https://doi.org/10.1016/j.jweia.2021.104609

[30] Chen C-W, Li Y-C, Lo Y-L. Interference effects on the square and circular cross-sectional high-rise buildings under turbulent flows. Inte J Archit Eng Tech. 2022; 9: 18-36. https://doi.org/10.15377/2409-9821.2022.09.2

[31] Counihan J. Simulation of an adiabatic urban boundary layer in a wind tunnel. Atmospheric Environment (1967) 1973; 7: 673-89. https://doi.org/10.1016/0004-6981(73)90150-9

[32] Taiwan Wind Code. Ministry of Interior 2015.

[33] Irwin HPAH, Cooper KR, Girard R. Correction of distortion effects caused by tubing systems in measurements of fluctuating pressures. J Wind Eng Ind Aerodyn. 1979; 5: 93-107. https://doi.org/10.1016/0167-6105(79)90026-6

[34] Quality assurance manual: Wind engineering studies of buildings. 3rd ed. Australian Wind Engineering Society; 2019, AWES-QAM-1-2019.

[35] Prévost JH, Bagrianski S. An introduction to matrix structural analysis and finite element methods. World Scientific; 2017. https://doi.org/10.1142/10358

[36] Uematsu Y, Watanabe K, Sasaki A, Motohiko Yamada, Hongo T. Wind-induced dynamic response and resultant load estimation of a circular flat roof. J Wind Eng Ind Aerodyn. 1999; 83: 251-61. https://doi.org/10.1016/S0167-6105(99)00076-8

[37] Uematsu Y, Yamada M. Wind-induced dynamic response and its load estimation for structural frames of circular flat roofs with long spans. Wind Struct. 2002; 5: 49-60. https://doi.org/10.12989/was.2002.5.1.049

[38] Uematsu Y, Moteki T, Hongo T. Model of wind pressure field on circular flat roofs and its application to load estimation. J Wind Eng Ind Aerodyn. 2008; 96: 1003-14. https://doi.org/10.1016/j.jweia.2007.06.025

[39] Simiu E, Yeo D. Wind effects on structures: modern structural design for wind. 4th ed. Wiley Blackwell; 2017.

[40] Chopra A. Dynamics of structures: theory and applications to earthquake engineering. 5th ed. Pearson; 2019.

[41] Clough R, Penzien J. Dynamics of structures. 2nd ed. McGraw-Hill; 1993.

[42] Newland D. Introduction to random vibrations, spectral & wavelet analysis. 3rd ed. Dover Publication Inc.; 1993.

[43] Holmes JD, Bekele SA. Wind loading of structures. 4th ed. CRC Press; 2020. https://doi.org/10.1201/9780429296123

[44] MacQueen J. Some methods for classification and analysis of multivariate observations. Proceedings of 5th Berkeley Symposium on Mathematical Statistics and Probability, University of California Press; 1967, p. 281-97.

[45] Huang Z. Extensions to the k-means algorithm for clustering large data sets with categorical values. Data Min Knowl Discov. 1998; 2: 283-304.

[46] Li Y, Yang Q, Tian Y, Zhu Y. Refinement analysis of multi-target equivalent static wind loads for large-span roofs. J Cent S Univ. 2016; 47: 2485-94.

[47] Scitovski R, Sabo K, Martínez-Álvarez F, Ungar Š. Cluster analysis and applications. Switzerland: Springer Cham; 2021. https://doi.org/10.1007/978-3-030-74552-3

[48] Tamura Y, Suganuma S, Kikuchi H, Hibi K. Proper orthogonal decomposition of random wind pressure field. J Fluids Struct. 1999; 13: 1069-95. https://doi.org/10.1006/jfls.1999.0242

[49] Kikuchi H, Tamura Y, Ueda H, Hibi K. Proper orthogonal decomposition study of fluctuating wind pressures acting on a tall building. J Struct Construction Engineering. J Struct Constr Eng. 1998; 63: 25-32. https://doi.org/10.3130/aijs.63.25_2